UNIABUJA Journal of Engineering and Technology

https://ujet.uniabuja.edu.ng/

ISSN: 2714-3236 (Online); 2714-3228 (Print)

Volume 3, Issue 1, 2026; 111-120

User-Friendly Control Mechanisms in Robotics Arm via Mobile Applications

Samuel OWOEYE[1]*, Folasade DURODOLA[2], Olufemi IPINNIMO[3], Ifeanyi UZODINMA[4], Francis ALI[5], Daniel AKINROTIMI[6]

[1,2,4,5,6]*Department of Mechatronics Engineering, Federal University of Agriculture, Abeokuta, Nigeria*
[3]*Department of System Engineering, University of Lagos, Lagos, Nigeria*

[1]*owoeyeso@funaab.edu.ng, [2]durodolafo@funaab.edu.ng, [3]oipinnimo@unilag.edu.ng, [4]uzodinmaiffy@gmail.com, [5]francisali692@gmail.com, [6]dtenny@gmail.com*

Abstract

Robotic arms have become an essential part of the manufacturing and non-manufacturing industries. They are in different forms and used to handle a variety of tasks. This research covers the development of an articulated 3R robotic arm controlled via an internet of things-enabled mobile application. The system features a 6-degree-of-freedom robotic arm constructed using MG996R servo motors, controlled by an ESP32 WROOM-32 microcontroller that enables wireless communication through Wi-Fi connectivity. A payload capacity of 100g, reach of 37.7 cm, and repeatability of ±2 mm was achieved, making it suitable for light industrial tasks such as pick-and-place operations, laboratory automation, and educational applications. The control interface consists of an intuitive mobile application that communicates with the ESP32, providing real-time control with an average latency of 45ms and enabling users to operate the arm without specialized robotics programming knowledge. When testing under no load conditions, the five joints responded within a range of 75ms to 150ms for 30° movement of the servo motor, 120ms to 200ms for 60° and 300ms to 600ms for a 90° movement. Tests were also carried out with a 100g load and a response range of range of 120ms to 270ms for 30° movement of the servo motor, 260ms to 360ms for 60° and 600ms to 1200ms for a 90° change. The mobile application was also tested to evaluate its performance. This showed a user interface response time of <50 ms for slider interactions and real-time feedback accuracy of ±1° position display accuracy.

Keywords: *Automation, ESP32, Microcontrollers, Servo motors, Wi-Fi Connectivity*.

1.0 Introduction

Robotic arms have become indispensable in modern industrial automation due to their flexibility, precision, and efficiency in performing repetitive and complex tasks (Aghili, 2022). Among these, articulated robotic arms with three revolute joints, commonly referred to as 3R robotic arms, hold particular significance for their ability to replicate human-like motion with reduced mechanical complexity. The emergence of low-cost microcontrollers, 3D printing technology, and internet of things (IoT) connectivity presents an opportunity to develop accessible robotic solutions without compromising essential functionality (Cameron, 2024; Chua & Leong, 2017). Internet of Things integration specifically enables remote monitoring and control capabilities that were previously available only in high-end systems, while mobile applications provide intuitive user interfaces that reduce the technical expertise required for operation (Jiang & Shi, 2019).

The growing interest in flexible process automation has created a demand for simple yet effective robotic solutions. High-end industrial robots, though effective, remain prohibitively expensive and difficult to integrate for startups and SMEs lacking the requisite technical and financial resources (Fan *et al.*, 2023). A major challenge in robotic arm design lies in accurate kinematic and dynamic modeling, essential for ensuring reliable movement and positioning. Moreover, robotic systems often require extensive reconfiguration to adapt to new tasks, making them inaccessible to non-expert users (Amirkhanov *et al.*, 2023).

Studies by Nguyen-Tuong and Peters (2011), Spong (2022) and Deng *et al.* (2023) provide key insights into robotic arm kinematics and dynamics. These works laid the groundwork for subsequent modeling techniques aimed at improving movement precision under varying conditions. However, the complexity of these models often hinders real-time implementation. Elhoseny *et al.* (2018) proposed an IoT framework for the real-time monitoring of industrial robots. This framework enabled remote monitoring and real-time data analysis to enhance operational efficiency. Nonetheless, the study mainly focused on monitoring, with limited discussion on the control and evaluation of the robotic arm. Jiang and Shi (2019) integrated IoT with robotic arms for smart manufacturing. Their research demonstrated improved adaptability and operational flexibility in robotic systems. However, their study focused on high-end industrial robots and did not address affordability for small and medium-sized enterprises (SMEs). Wang *et al.* (2020) developed an IoT-

Received: 27-12-2025 / Accepted: 05-01-2026 / Published: 29-01-2026

https://doi.org/10.70118/ujet.2026.0301.11

based control system aimed at enhancing robotic safety and predictive maintenance. Their system showed how real-time data could improve safety and extend system longevity. Despite these benefits, the scope of their work was limited in terms of controlling multiple robotic arms across a large-scale production network.

This paper presents the design, construction, and evaluation of a 3R robotic arm with six DOF, remotely controlled via a custom-built IoT mobile application. This work represents a scalable prototype adaptable for use in industrial and educational settings. The arm is engineered to perform general-purpose operations such as pick-and-place tasks while remaining adaptable through an API-exposed control interface. The dual-phase project design encompasses both hardware (mechanical frame and electronics) and software (firmware and mobile app) components. Significantly, this research highlights the potential for democratizing automation by focusing on intuitive control mechanisms and modular expandability.

2.0 Materials and Methods

A structured, iterative development process was followed, beginning with mechanical design and proceeding to hardware integration and software development. The methodology ensured each subsystem was tested and validated independently before full system integration. The system's block diagram as shown in Figure 1, details the interactions between the ESP32 microcontroller, power supply, servo motors, sensors, and the mobile application. It provides a holistic view of data and signal flow across system modules.

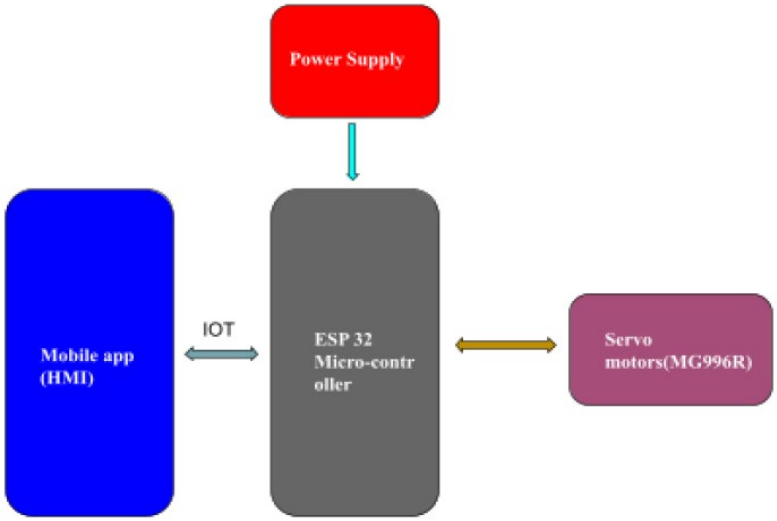

Figure 1: Block diagram of the system

The operational flow chart outlines logical steps from user interaction with the mobile application to the physical movement of the robotic arm. Figure 2 shows the flowchart which captures initialization, command parsing, servo actuation, and error handling routines.

Received: 27-12-2025 / Accepted: 05-01-2026 / Published: 29-01-2026

https://doi.org/10.70118/ujet.2026.0301.11

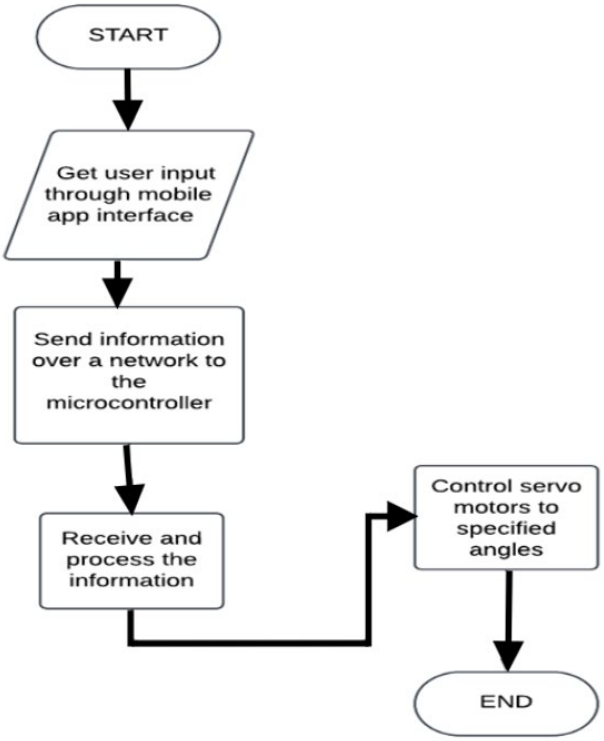

Figure 2: System functional flowchart

2.1 Hardware components

2.1.1 ESP32 WROOM microcontroller

Selected for its dual-core processing and built-in wireless communication (Wi-Fi and Bluetooth), the ESP32 MCU as shown in Figure 3 is the project's control hub. Its extensive GPIO availability accommodates multiple servo connections, and its cost-efficiency makes it ideal for low-budget applications.

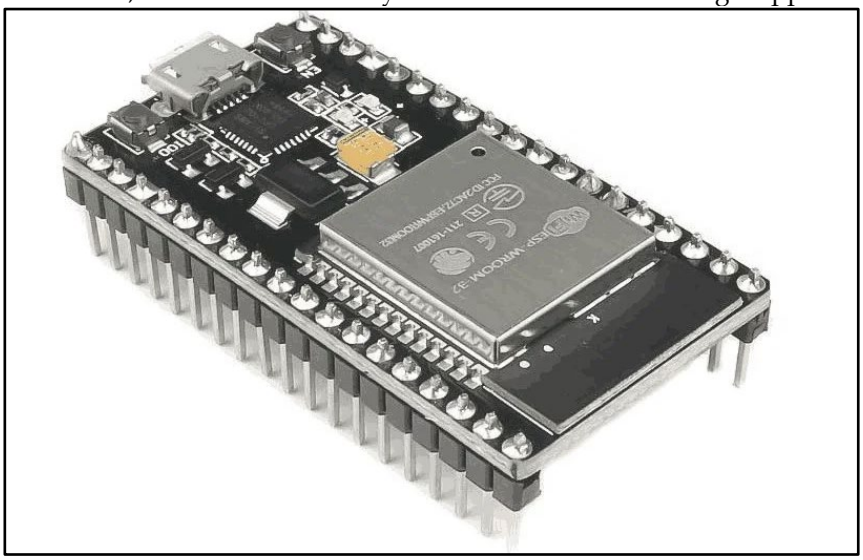

Figure 3: ESP32 WROOM Development Board

2.1.2 MG996R servo motors

The robotic arm is actuated by MG996R digital servo motors. Figure 4 shows the servo motors, chosen for their reliability, torque output, and metal gear construction, six servo motors were used to support the six degrees of freedom required by the articulated design.

Received: 27-12-2025 / Accepted: 05-01-2026 / Published: 29-01-2026

https://doi.org/10.70118/ujet.2026.0301.11

2.2 Software and control design

The software comprises two key parts: firmware for the ESP32 and the mobile control interface. The firmware was developed in C++ using Arduino IDE and ESP-IDF, the firmware handles wireless connectivity,

Figure 4: MG966R Servo motor

MQTT-based messaging, and servo control logic, while the Mobile App was developed using Flutter, the app features an intuitive user interface with sliders and buttons for controlling each servo motor independently.

2.3 Design calculations

2.3.1 Forward kinematics:

The forward kinematics describes the position of the end effector given specific values of the joint parameters. The Denavit-Hartenberg (D-H) convention is a standardized method for representing robotic manipulators using four parameters: link length (a_i), link twist (α_i), joint offset (d_i), and joint angle (θ_i). These parameters define the transformation between consecutive frames, simplifying kinematic analysis.

Transformation matrix for each joint is shown in equation 1 (Owoeye *et al.*, 2024)

$$T_{i-1}^{i} = \begin{bmatrix} \cos\theta_i & -\sin\theta_i \cos\alpha_i & \sin\theta_i \sin\alpha_i & a_i \cos\theta_i \\ \sin\theta_i & \cos\theta_i \cos\alpha_i & -\cos\theta \sin\alpha_i & a_i \sin\theta_i \\ 0 & \sin\alpha_i & \cos\alpha_i & d_i \\ 0 & 0 & 0 & 1 \end{bmatrix} \quad (1)$$

The D-H parameters for the 3R robot and its end effector (3R) is shown in Table 1 with all parameters retaining their usual meanings

Table 1: D-H parameters for the robotic arm

Links	$\boldsymbol{\alpha_{i(\mathrm{deg})}}$	$\boldsymbol{a_i}$	$\boldsymbol{d_i}$	$\boldsymbol{\theta_{i(deg)}}$
0-1	90	0	d_1	θ_1
1-2	0	a_2	0	θ_2
2-3	0	a_3	0	θ_3
3-4	90	a_4	0	θ_4
4-5	-90	0	d_2	θ_5
5-6	0	a_6	d_3	θ_6

The transformations matrix for each link using the DH parameter are shown in equations 2- 7:

$$T_0^1 = \begin{bmatrix} \cos\theta_1 & 0 & \sin\theta_1 & 0 \\ \sin\theta_1 & 0 & -\cos\theta_1 & 0 \\ 0 & 1 & 0 & d_1 \\ 0 & 0 & 0 & 1 \end{bmatrix} \quad (2)$$

Received: 27-12-2025 / Accepted: 05-01-2026 / Published: 29-01-2026

https://doi.org/10.70118/ujet.2026.0301.11

$$T_1^2 = \begin{bmatrix} \cos\theta_2 & -\sin\theta_2 & 0 & a_2\cos\theta_2 \\ \sin\theta_2 & \cos\theta_2 & 0 & a_2\sin\theta_2 \\ 0 & 0 & 1 & 0 \\ 0 & 0 & 0 & 1 \end{bmatrix} \quad (3)$$

$$T_2^3 = \begin{bmatrix} \cos\theta_3 & -\sin\theta_3 & 0 & a_3\cos\theta_3 \\ \sin\theta_3 & \cos\theta_3 & 0 & a_3\sin\theta_3 \\ 0 & 0 & 1 & 0 \\ 0 & 0 & 0 & 1 \end{bmatrix} \quad (4)$$

$$T_3^4 = \begin{bmatrix} \cos\theta_4 & 0 & \sin\theta_4 & a_4\cos\theta_4 \\ \sin\theta_4 & 9 & -\cos\theta_4 & a_4\sin\theta_4 \\ 0 & 1 & 0 & 0 \\ 0 & 0 & 0 & 1 \end{bmatrix} \quad (5)$$

$$T_4^5 = \begin{bmatrix} \cos\theta_5 & 0 & -\sin\theta_5 & 0 \\ \sin\theta_5 & 0 & \cos\theta_5 & 0 \\ 0 & -1 & 0 & d_5 \\ 0 & 0 & 0 & 1 \end{bmatrix} \quad (6)$$

$$T_5^6 = \begin{bmatrix} \cos\theta_6 & -\sin\theta_6 & 0 & a_6\cos\theta_6 \\ \sin\theta_6 & \cos\theta_6 & 0 & a_6\sin\theta_6 \\ 0 & 0 & 1 & d_6 \\ 0 & 0 & 0 & 1 \end{bmatrix} \quad (7)$$

The final transformation from the end effector to the base frame is given by the multiplication of the 6 matrices above, as shown in equation 8:

$$T_0^6 = T_0^1 T_1^2 T_2^3 T_3^4 T_4^5 T_5^6 \quad (8)$$

2.3.2 Inverse kinematics

Inverse kinematics involves determining the joint parameters (θ_1,θ_2,θ_3,θ_4 ,θ_5,θ_6) required to achieve a desired end-effector position and orientation. Given the homogeneous transformation matrix of the end-effector, we compute the joint angles systematically. The end-effector pose is represented by the transformation matrix in equation 9

$$T_6^0 = \begin{bmatrix} r_{11} & r_{12} & r_{13} & P_x \\ r_{21} & r_{22} & r_{23} & P_y \\ r_{31} & r_{32} & r_{33} & P_Z \\ 0 & 0 & 0 & 1 \end{bmatrix} \quad (9)$$

Where:

- P_x, P_y, P_z define the end-effector position
- r_{ij} represents the orientation from the rotation matrix.

The first joint angle which controls the rotation about the Z-axis was determined using equation 1

$$\theta_1 = atan2(P_y,\ P_x) \quad (10)$$

The distance from the base to the end effector coordinate was derived using Pythagorean theorem as shown in equation 11

$$r = \sqrt{P_x^2 + P_y^2} \quad (11)$$

The effective height z

$$z = P_z - d_1 \quad (12)$$

The various links angles are calculated using equations 13 to 17

$$Cos\ \theta_3 = \frac{r^2 - L_2^2 - L_3^2}{2\ L_2\ L_3} \quad (13)$$

$$\theta_2 = atan2\ (2, r) - atan2(L_3 \sin(\theta_3)\ L_2 + L_3 \cos(\theta_3)) \quad (14)$$

$$\theta_4 = atan2\ (r_{32}, r_{33}) \quad (15)$$

Received: 27-12-2025 / Accepted: 05-01-2026 / Published: 29-01-2026

https://doi.org/10.70118/ujet.2026.0301.11

$$\theta_5 = atan2\left(\sqrt{r_{31}^2} + r_{32}^2, r_{33}^2\right) \quad (16)$$

$$\theta_6 = atan2(r_{21}, r_{11}) \quad (17)$$

2.4 Repeatability

Repeatability is the robot's ability to return to the same pose (position and/or orientation) under identical conditions (Russo, 2022; Amanov *et al.,* 2021; Alahmed *et al.,* 2025). Firstly, a defined target position was established within the operational workspace of the robotic arm. This position is chosen based on the arm's range of motion and is marked for reference (Mourtzis *et al.,* 2022; Rong *et al.,* 2025).

The arm is then programmed to move to this target position multiple times under the same operational conditions, ensuring that variables such as load, environment, and control parameters remain constant. It was then controlled to reach the designated target position, and the position of the end effector is measured using a laser rangefinder. For each movement, the actual position of the end effector is recorded. The repeatability is then expressed as a range or an interval, typically reported in millimeters, indicating the maximum deviation from the target position.

2.5 Torque and power analysis

In conducting a static force analysis for the robotic arm, the torque required at Joint 2 (the shoulder) when the arm is fully extended with a 100g payload was calculated using equation 18.

$$\tau = F \times L \quad (18)$$

where F is the weight of the payload, the distance from Joint 2 to the point of the payload application is L, the torque τ.

The MG996R servo motor, which powers Joint 2, boasts a torqe rating of approximately 9.4 kg-cm, equivalent to about 0.93 Nm when operating at standard voltage, indicating that the motor has enough torque capacity to handle the load comfortably under ideal conditions.

Factors such as power supply fluctuations, mechanical friction, and the inertia of the arm can lead to situations where the effective torque drops, thereby increasing the risk of stalling when the servos struggle to provide sufficient power to maintain movement or positioning against the gravitational forces acting on the payload. Additionally, sustained operation at higher load limits can result in thermal buildup within the motors, further reducing their performance.

3.0 Results and Discussion

A variety of tests were performed to ensure the system operated optimally and evaluate the current limitations of the robot. These included:

3.1 No-Load operation performance

Individual joint testing under no-load conditions revealed consistent performance characteristics across all six degrees of freedom. Table 2 presents the angular traverse times for each joint across the tested angular ranges while Figure 5 shows a graph of traversal time (ms) against angle, under no-load conditions. The results demonstrated a relationship between angular displacement and traverse time, consistent with servo motor acceleration and deceleration profiles. Base rotation (Joint 0) exhibited the fastest response times due to minimal mechanical load, while the primary arm joints (Joints 1 and 2) showed increased traverse times reflecting their load-bearing responsibilities.

Table 2: Angular traverse time for each joint under no-load conditions.

Angle	Arm/Joint 1 (ms)	Arm/Joint 2 (ms)	Base yaw/Joint 0 (ms)	End effector roll/Joint 3 (ms)	End effector pitch/Joint 4 (ms)
0 to 30	150	100	80	65	75
0 to 60	200	178	140	120	130
0 to 90	600	480	430	380	300

Received: 27-12-2025 / Accepted: 05-01-2026 / Published: 29-01-2026

https://doi.org/10.70118/ujet.2026.0301.11

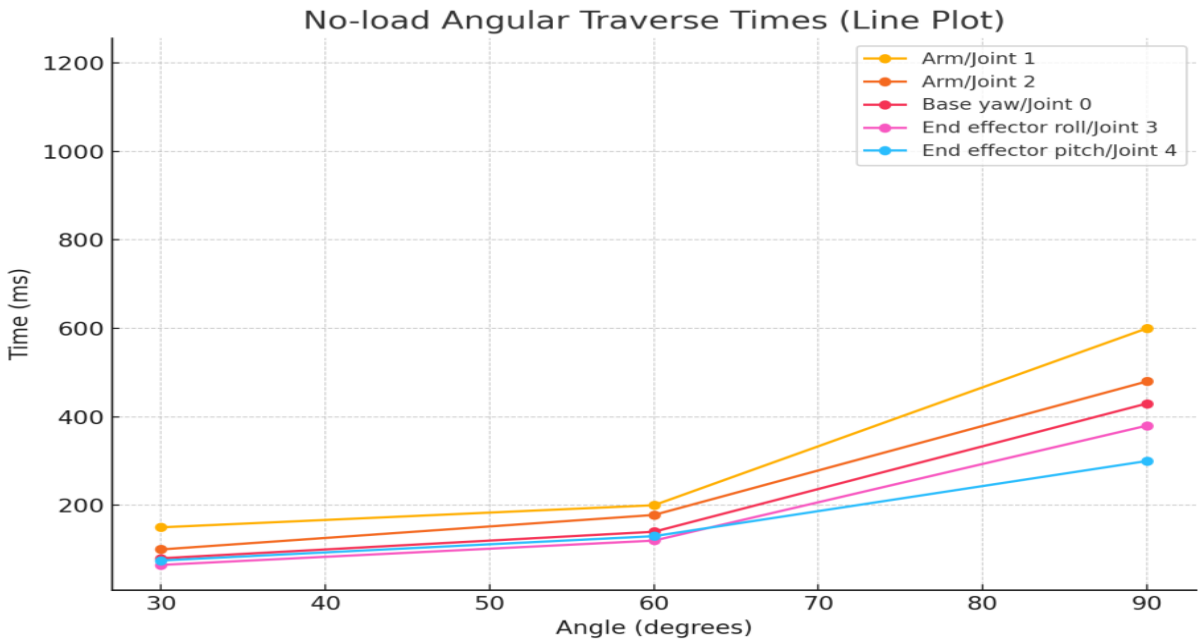

Figure 5: A graph of traversal time (ms) against angle, under no-load conditions

3.2 Loaded operation performance

Testing under 100g payload conditions showed predictable performance degradation across all joints. Table 3 summarizes the loaded operation results while Figure 6 shows a graph of traversal time (ms) against angle, under a 100g load condition. The payload testing revealed performance degradation ranging from 50% to 100% increase in traverse times, with the most significant impact observed on the primary load-bearing joints (Joints 1 and 2). This performance degradation is within acceptable limits for educational and light industrial applications.

Table 3: Angular traverse time for each joint under 100g load

Angle	Arm/Joint 1 (ms)	Arm/Joint 2 (ms)	Base yaw/Joint 0 (ms)	End effector roll/Joint 3 (ms)	End effector pitch/Joint 4 (ms)
0 to 30	270	200	160	120	140
0 to 60	360	320	280	240	260
0 to 90	1200	960	860	760	600

Received: 27-12-2025 / Accepted: 05-01-2026 / Published: 29-01-2026
https://doi.org/10.70118/ujet.2026.0301.11

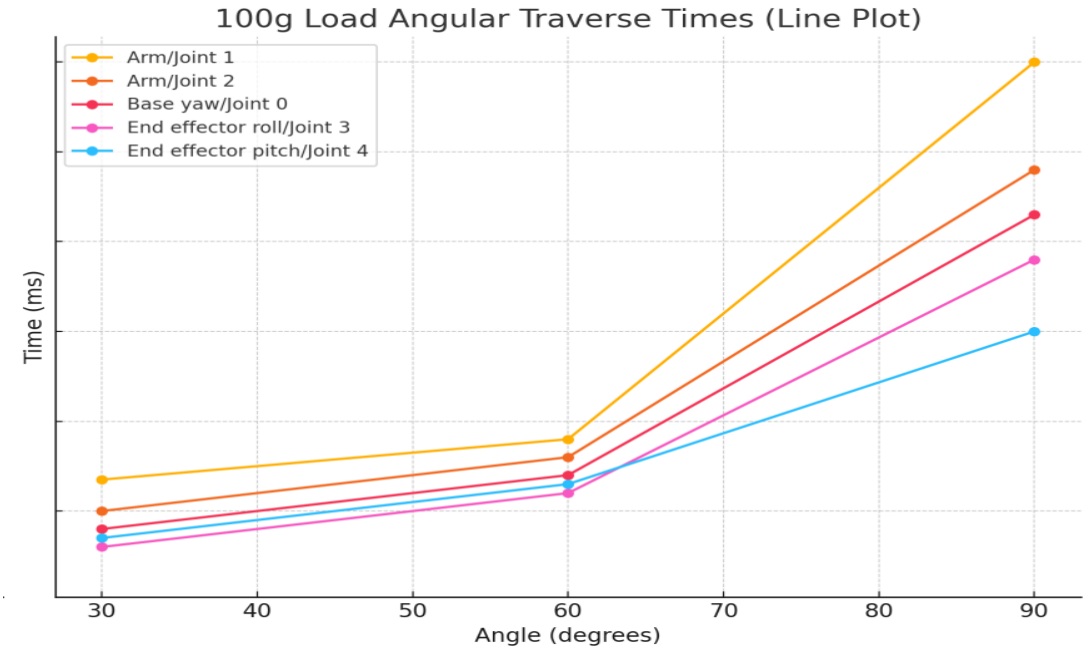

Figure 6: A graph of traversal time (ms) against angle, under ideal load (100g) conditions.

Comparing Tables 1 and 2 revealled that there is a longer response time to reach the same angle when a load is being carried by the arm. This is because the servo motors have to do more work when carrying a load. Figure 7 which shows the finished robotic arm and depicts the configuration of each joint and their relative positions to each other.

Figure 7: Completely assembled arm

3.3 System integration performance

Comprehensive positioning tests conducted across the workspace of the 3R articulated robotic arm yielded several important performance characteristics. The positioning repeatability was measured at ±2 mm, indicating a high level of precision in the arm's movements. The maximum reach of the robotic arm was validated at 37.7 cm, confirming its capability to extend effectively within this range. Additionally, the spherical workspace radius was confirmed to be 37 cm, demonstrating the arm's versatility in accessing various points within its operational area. Notably, the robotic arm also exhibited a full 360° rotation capability during horizontal sweeps, enhancing its manoeuvrability and allowing for comprehensive coverage of its workspace. These performance characteristics collectively affirm the robotic arm's effectiveness and reliability in executing tasks within its designated environment.

Received: 27-12-2025 / Accepted: 05-01-2026 / Published: 29-01-2026

https://doi.org/10.70118/ujet.2026.0301.11

3.4 Mobile application performance

The mobile application interface shown in Figure 8, demonstrated excellent responsiveness and functionality. The user interface response time is less than 50 milliseconds during slider interactions, which ensures a seamless user experience and control. Additionally, the real-time feedback accuracy maintains a ±1° position display accuracy, allowing for precise monitoring of the arm's movements. Feature reliability is crucial and a 100% success rate was achieved for all implemented functions, ensuring that every command executed by the robotic arm performs as intended without failure. Finally, the command execution time ranged between 45 to 200 milliseconds, depending on network conditions, providing timely responses to user inputs while accommodating variations in network performance. These key performance indicators collectively contribute to the overall effectiveness and reliability of the robotic arm in various applications.

During extensive testing of the developed 3R articulated robotic arm, several operational limitations were identified and characterized. One major issue pertains to connectivity, where network congestion significantly impacts performance, particularly when multiple devices share the same Wi-Fi network. Under high network traffic conditions, delays in MQTT communication can exceed 200 milliseconds, leading to sluggish response times. Additionally, the communication range is limited to approximately 20 meters in typical indoor environments, which restricts operational flexibility and usability.

Power management also emerged as a critical limitation. The motors, when under full load, draw up to 2 amps of total current, necessitating a stable power supply with a capacity of at least 10 amps for reliable operation. Furthermore, voltage fluctuations can adversely affect servo positioning accuracy and response times, with motors stalling if inadequate power is supplied. These limitations highlight the need for improvements in both connectivity and power management to enhance the overall performance and reliability of the robotic arm in practical applications.

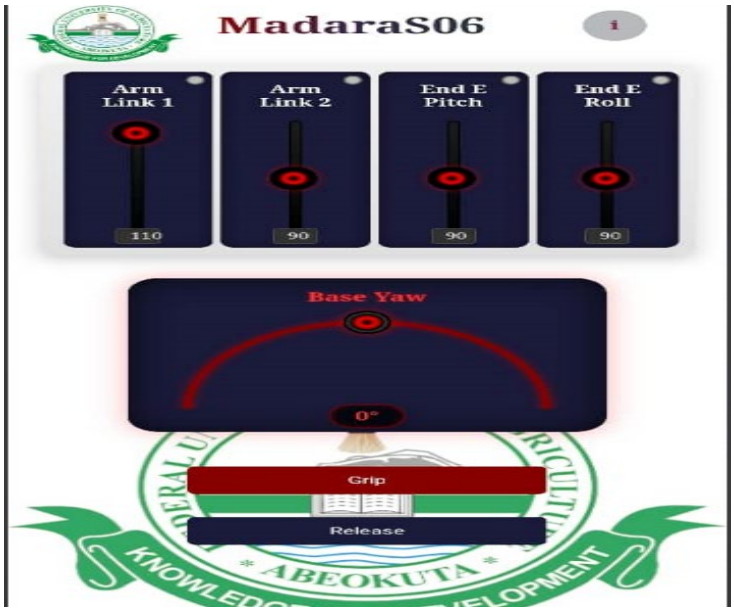

Figure 8: Mobile application control interface (HMI)

4.0 Conclusion

As proposed, the 3R robotic arm which was developed mainly for control via a mobile application was developed. The robotic arm worked perfectly with the built mobile application interface. The mobile application serves as a Human-Machine Interface (HMI) which allows intuitive interactions from the user. This HMI communicates wirelessly with the ESP32 microcontroller through Wi-Fi connectivity. This enables the mobile application to be accessed through any Wi-Fi-connected mobile device, providing accessibility and ease of use for the end user. The forward kinematics functionality can be specified through the app to perform proper operation, enabling users to control the arm through direct joint control.

References

Aghili, F. (2022). Self-tuning multi-arm coordination for cooperative robot manipulators. *Robotica*, 40(6), 1805–1819.

Alahmed, F., Hawwa, M., & Baroudi, U. (2025). Development of an Autonomous Robot for Precision Floor Marking. *Robotics*, *15*(1), 7.

Received: 27-12-2025 / Accepted: 05-01-2026 / Published: 29-01-2026

https://doi.org/10.70118/ujet.2026.0301.11

Amanov, E., Nguyen, T. D., & Burgner-Kahrs, J. (2021). Tendon-driven continuum robots with extensible sections—A model-based evaluation of path-following motions. *The International Journal of Robotics Research*, *40*(1), 7-23.

Amirkhanov, R., Vasilev, A., Ibragimov, A., & Klimov, D. (2025). ESP32-MQTT based real-time control system for robotic operations. *In 2025 2nd International Conference on Artificial Intelligence, Big Data and Information Technology (AIBIT*) (pp. 1-6). IEEE.

Cameron, H. R., Castle-Green, S., Chughtai, M., Dowthwaite, L., Kucukyilmaz, A., Maior, H. A., & Stahl, B. C. (2024). A Taxonomy of Domestic Robot Failure Outcomes: Understanding the impact of failure on trustworthiness of domestic robots. *In TAS '24: The 2024 Conference on Trustworthy Autonomous Systems* (pp. 1-10).

Chua, B. L., & Leong, K. C. (2017). A review of robotics education with a focus on the use of robotics kits. *Journal of Educational Technology & Society,* 20(2), 12-23.

Deng, L., Xu, B., Gao, Z., Miao, M., Hu, C., & Song, A. (2023). Decoding natural grasping behaviors: Insights into MRCP source features and coupling dynamics. *IEEE Transactions on Neural Systems and Rehabilitation Engineering*, *31*, 4965-4976.

Elhoseny, M., Abdelaziz, A., Salama, A. S., Riad, A. M., Muhammad, K., & Sangaiah, A. K. (2018). A hybrid model of Internet of Things and cloud computing for improved services in smart cities. *Future Generation Computer Systems*, 86, 734-742.

Fan, Z., He, X., Xu, X., & Liu, Y. (2023). A review of modeling and control of continuum robots. *Advanced Intelligent Systems,* 5(5), 2200367.

Jiang, Y., & Shi, D. (2019). Design and research on the control system of sorting robots based on machine vision. *In 2019 11th International Conference on Measuring Technology and Mechatronics Automation (ICMTMA)* (pp. 569-572). IEEE.

Mourtzis, D., Angelopoulos, J., & Panopoulos, N. (2022). Closed-loop robotic arm manipulation based on mixed reality. *Applied sciences*, *12*(6), 2972.

Nguyen-Tuong, D., & Peters, J. (2011). Model learning for robot control: a survey. *Cognitive processing*, *12*(4), 319-340.

Rong, J., Liu, Y., Li, X., Gao, C., Wang, P., Yuan, T., & Li, W. (2025). Decoupled motion planning method for 7-DOF manipulator and lifting joint in automated tomato harvesting. *Computers and Electronics in Agriculture*, *237*, 110693.

Russo, M. (2022). Measuring performance: Metrics for manipulator design, control, and optimization. *Robotics*, *12*(1), 4.

Spong, M. W. (2022). An historical perspective on the control of robotic manipulators. *Annual review of control, robotics, and autonomous systems*, *5*(1), 1-31.

Wang, L., Wang, X. V., & Gao, L. (2020). A systematic review of robotic technologies in fighting against COVID-19. *Journal of Manufacturing Systems,* 57, 454-467.

Received: 27-12-2025 / Accepted: 05-01-2026 / Published: 29-01-2026
https://doi.org/10.70118/ujet.2026.0301.11